IConTES 2024: International Conference on Technology, Engineering and Science

Temperature Effect on the Creep Behavior of the Upstream Bituminous Concrete Masks of the Bouhnifia Dam

Ghouilem Kamel
University Mouloud Mammeri of Tizi – Ouzou

Atlaoui Djamal
University Mouloud Mammeri of Tizi – Ouzou

Merakeb Seddik
University Mouloud Mammeri of Tizi – Ouzou

Mehaddene Rachid
University Mouloud Mammeri of Tizi – Ouzou

Abstract: This paper, presents creep behavior of the concrete bituminous and it evolution under three different temperatures (17°C, 32°C, and 40°C) and their effect on the stress curves evolution at the upstream mask in the bouhnifia dam (Algeria), who is considered a rock fill dam of 55m high sealed by an upstream sealing mask in bituminous coating 20 cm thick. Creep is a time-dependent deformation resulting from constant load who is characterized by a nonlinear behavior of the materials, in which the material continues to become deform under a constant load. In this study, we have applied the Finite Element Method based on a model called (Time Hardening Model) using the computer code ANSYS 17.0 in order to simulate a creep behavior of the upstream mask during 20000 hours of loading and the evolution stress curves under three different temperatures (17°C, 32°C, and 40°C) successively. First, we simulate the temperature distribution in transient conditions during a day of sunshine on the facing, and then we evaluate the creep behavior of the mask under different temperatures mentioned above.

Keywords: Concrete bituminous, Finite element method, Creep, Ansys, Temperatures

Introduction

The performance of bitumen in terms of waterproofing has been known since Antiquity. Today we see hydraulic structures based on bitumen 3000 years old, such as the dikes of the Tigris, in Assur, in Mesopotamia still in good condtion (Djemili & Chiblak, 2007; Chebbah 2020). Bituminous coatings are waterproof, durable, insensitive to water, resistant to most common chemical agents and micro-organisms, they have a great ability to solve many hydraulic problems; the flexibility of bituminous waterproofing allows them to adapt to the settlement of their support without cracking or losing their properties (Lombari, 2005; Djemili et al., 2012).

Asphalt concrete provides waterproofing for dams, and it can be use on any inclination of the embankment dam, where it has the capacity to take the movement of the foundation without any loss of waterproofing, due to its sufficient flexibility. Asphalt concrete layers have enough durability due to the low air content in the compacted layers, which reduces the effect of climate on these layers (Fadel, 2005). The ambient temperatures air influence directly the structure temperatures, while atmospheric conditions (solar radiation, UV radiation, clouds, etc.) can accentuate these phenomena (Rychen, 2013; Chebbah, 2021). The mechanical properties of asphalt concrete change significantly with temperature. Surface heat transfer produces high stress gradients near the mask

surface, diurnal temperature cycles can induce fatigue cracking and reeze-thaw cycles can cause cracks (Mauduit et al., 2013; Chebbah, 2021). In this study we consider a rock fill dam of 55m high sealed by an upstream sealing mask in bituminous coating 20 cm thick see Figure 1. First, we simulate the temperature distribution in transient conditions during a day of sunshine on the facing, and then we evaluate the creep behavior of the mask under different temperatures mentioned above.
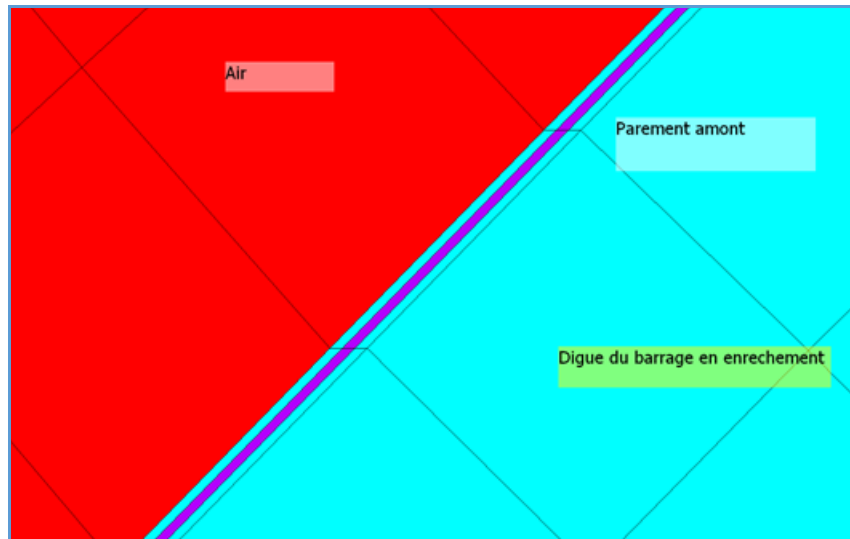

Figure 1. Upstream mask modeling

Materials and Method

Based on the existing documentation at the level of the National Agency for Dams and Transfer (ANBT), the data collection is summarized as follows: The waterproof mask is composed of a support layer (binder) 10 cm thick on which are applied one or two layers of 10 cm thick each of waterproof bituminous concrete (bitumen content: 7 to 9%, index of empty < 3%. The upstream mask includes the important details, such as :

- Climatic sun protection "mastic",
- 10 cm of waterproof asphalt concrete,
- 8 cm de bituminous drain,
- 10 cm of waterproof asphalt concrete,
- Binding layer,

Case Study

Figure 2, illustrate an dam overview which constitutes a basic model of the case study. The Bouhanifia dam located in western Algeria, at 02°35'9 37''E of longitude and 36°9' 19.06"N of latitude. The dam structure is made by a secured rock embankment on which an upstream sealing mask of bituminous concrete is placed. It is a rock fill dam with an upstream bituminous concrete mask, inspired dy the Ghrib dam. Built between 1930 and 1941, the Bouhnifia dam is among the first rock-fill structures made with an upstream bituminous concrete mask (Djemili, 2006; Ghouilem, 2014). The study site is characterized by a semi-arid climate. The dam watershed has an area of 7,850 km^2 and the average annual flow reached 110.106 m^3. The structure dam is characterized by:

- Peak length : 464 m,
- Height above the talweg : 55 m,
- Crown width : 5 m,
- Fruit of the slope variable upstream: 0,8/1 à 1/2,
- Fruit of the slope downstream : 1,25/1,
- Base massif width: 137 m,
- Dam capacity: 72.106m^3.

Figure 2. Overview of the Bouhnifia dam

Structural Discretization

The finite element Analysis (FEA) method is a powerful computational technique for approximate solutions. Several software programs adopt it, in particular the Anysy calculated code. The graphical user interface (GUI) allows us to model the finite element structure, as shown in figure 4. Elements PLANE 55 are used to discretize the upstream mask. They are designe for heat transfert problems. The structure dam is modeled by the elements PLANE 183 with eight nodes, see figure 3. Figure 4 illustrat the structure discretization by the elements PLANE 183.
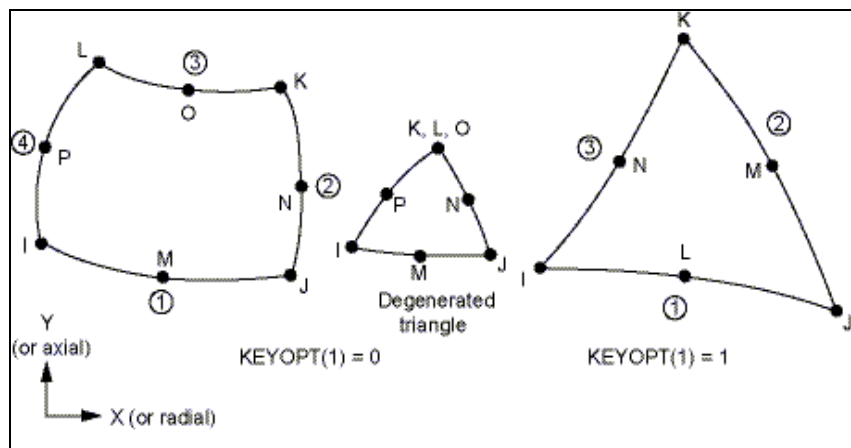

Figure 3. Elements PLANE183 (ANSYS Element Reference)

Temperature Evolution on the Mask Surface

The upstream mask structure is made up of layers of different nature and different thermal characteristics (see figure 2 above). In the study, we assume the following conditions:

- The structure temperature is not influenced by the heat input from the bituminous coating layer at a 1m of depth,
- The different structure layers are considered isotropic and homogeneous,
- The wind speed is constant over the entire period.
- There is conservation of flow at every massif point,
- The solar radiation acts only on the surface. It therefore does not constitute an internal source of heat

In reality, the upstream mask surface is subjects to the acts of solar radiation and convection of the surrounding atmosphere. They will be considered as boundary conditions. The heat quantity emitted or absorbed by the radiation thermal between the surface and the surrounding environment is given by the following equation (1) (Incropera et al., 2002).
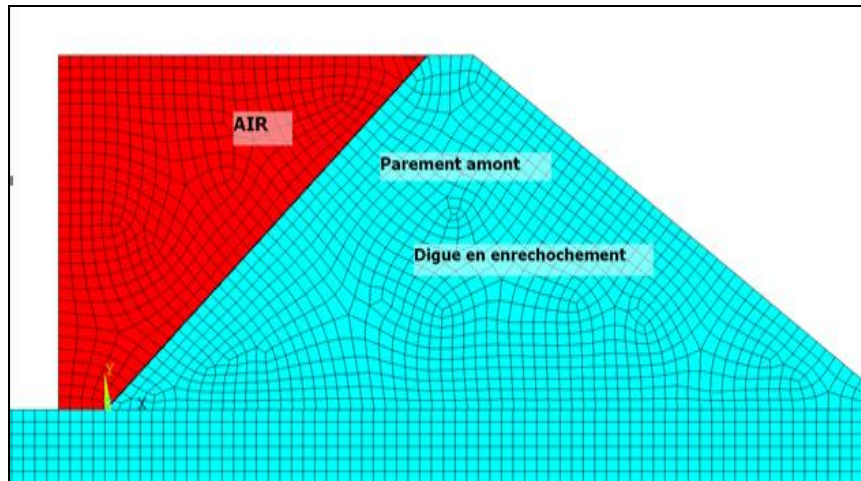

Figure 4. Structure discretization by the elements PLANE 183

$$q_{rad} = \varepsilon_s C_s (T_s^4 - T_{air}^4) \qquad (1)$$

With: $qrad$ is Radiation heat flux (W/m²), ε_s is the emission surface coefficient (εs =1 for a black body, and 0.85< εs < 0.95 for a bituminous concrete), **Cs** is the stephan-Boltzmann constant (Cs=5.67 .10−8 w $/m$ 2 °C⁴), **Ts** represent the mask surface temperature (°C) and $Tair$ is the air temperature (°C). The modeling evolution of temperature for each layers mask is given by the following thermal field equation：

$$\frac{\partial^2 T_i}{\partial X^2} - \frac{1}{a_i} \frac{\partial T_i}{\partial t} = 0 \qquad (2)$$

with: $a = \lambda/\rho.c$ is the thermal diffusivity (propagation coefficient heat), λ : Conductivity heat coefficient (w/m.k), ρ : Density (kg/m³),and **c** is the specific heat (j/kg.°C). The following empirical equation (3) giving by (George KP & Husain S, 1986), estimate the surface temperature evolution (Ts) of the coating depending on the ambient air temperature.

$$T_s = T_{air}\left(1 + \frac{76.2}{h_1 + 304.8}\right) - \frac{84.7}{h_1 + 304.8} + 3.3 \quad (3)$$

With: **T$_s$** is the surface coating temperature, **T$_{air}$**: Air temperature, **h$_1$**: bituminous layer thickness in cm. The following Table 1 illustrates the temperature (Ts) maximal results achieved on the surface of upstream mask using equation (3) above:

Table 1. Temperature evaluation (Ts) on the mask surface

Temperature Air (Tair)	17°C	32°C	40°C
Ts	27°C	43°C	54°C

The following Figures 5 bellow, illustrates the daily variation temperature (17°C, 32°C and 40°C) as a function of time (t) on the mask surface. For the ambient temperature air of 17°C, we note that the maximal temperature reached at the upstream mask surface is 31°C during 6h30' of exposure to the radiation solar. The evolution temperature of 32°C over time reached a pic of 60°C after 4h of exposure to solar radiation. Finally a maximal temperature of 65°C is reached on the surface upstream mask for the transient evolution of the temperature 40°C after 3h of exposure to the radiation solar. We note that from these results, the maximum temperatures reached on the surface mask are inversely proportional to the solar radiation time exposure. Figures 6, illustrates the variation daily temperature (17°C, 32°C andt 40°C) depending on the mask depth. These curves are obtained by the Fourier law (d²T/dx²= dTi/a$_i$.dt). Table 2 bellow illustrates the surface temperature evolution.(Ts) as a

function of the mask depth according to equation (3) and the temperature obtained by Ansys simulation. Through the results obtained concerning the surface temperature (Ts), that there is a significant difference between the Ansys simulation and the empirical equation (3). This can allow us to conclude that this equation does not take into account time of exposure to solar radiation.
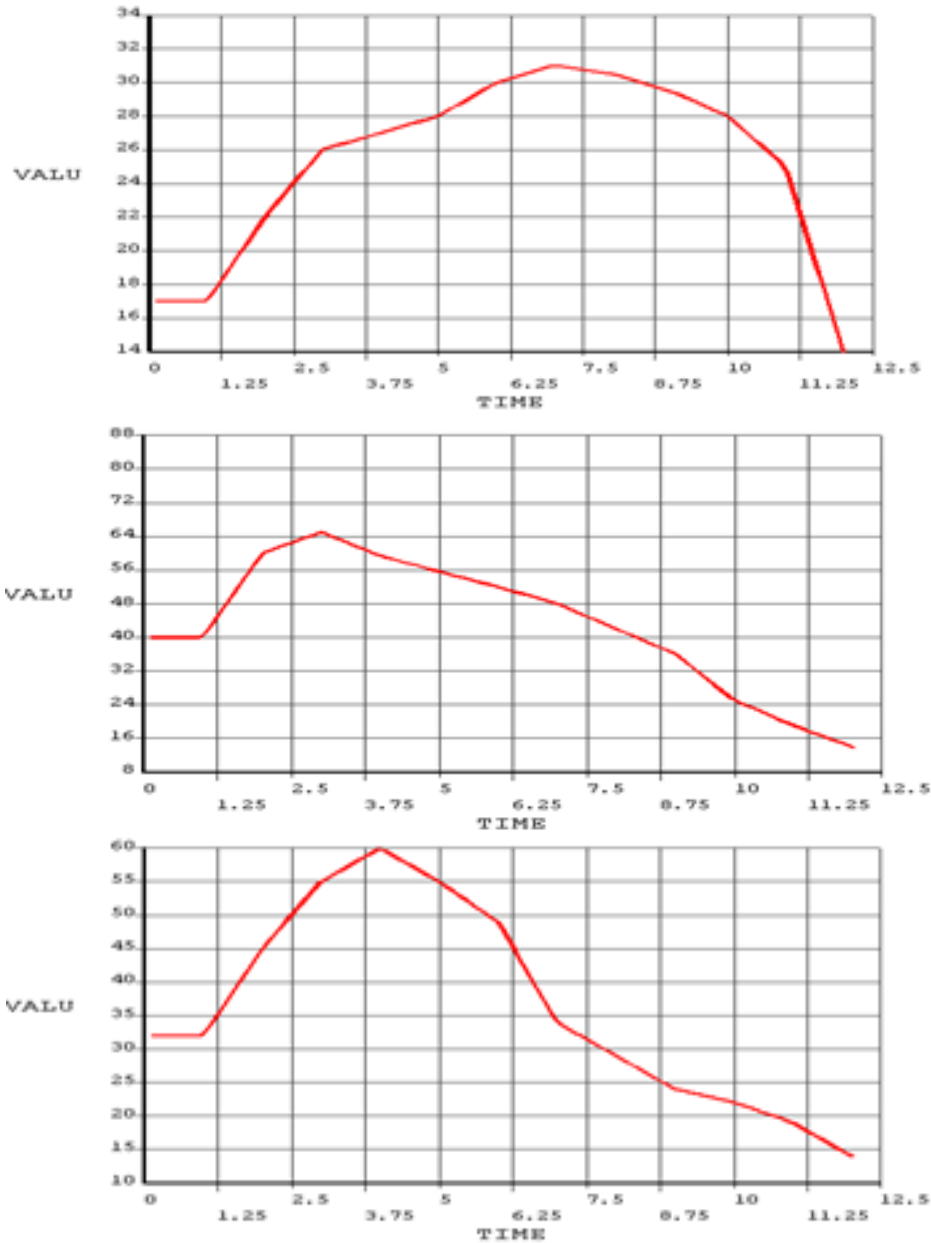

Figure 5. Temperatures evolution on the upstream ask

Creep Modeling Procedure by Ansys

Implicit creep is the most used method in the Ansys program for the reasons of efficiency. The command TB with Lab = CREEP allows us to programme this method and choose the corresponding equation creep by specifying the number of the model that it corresponding by using the TBOPT command, see example below.

TB, CREEP, 1,1,4,2
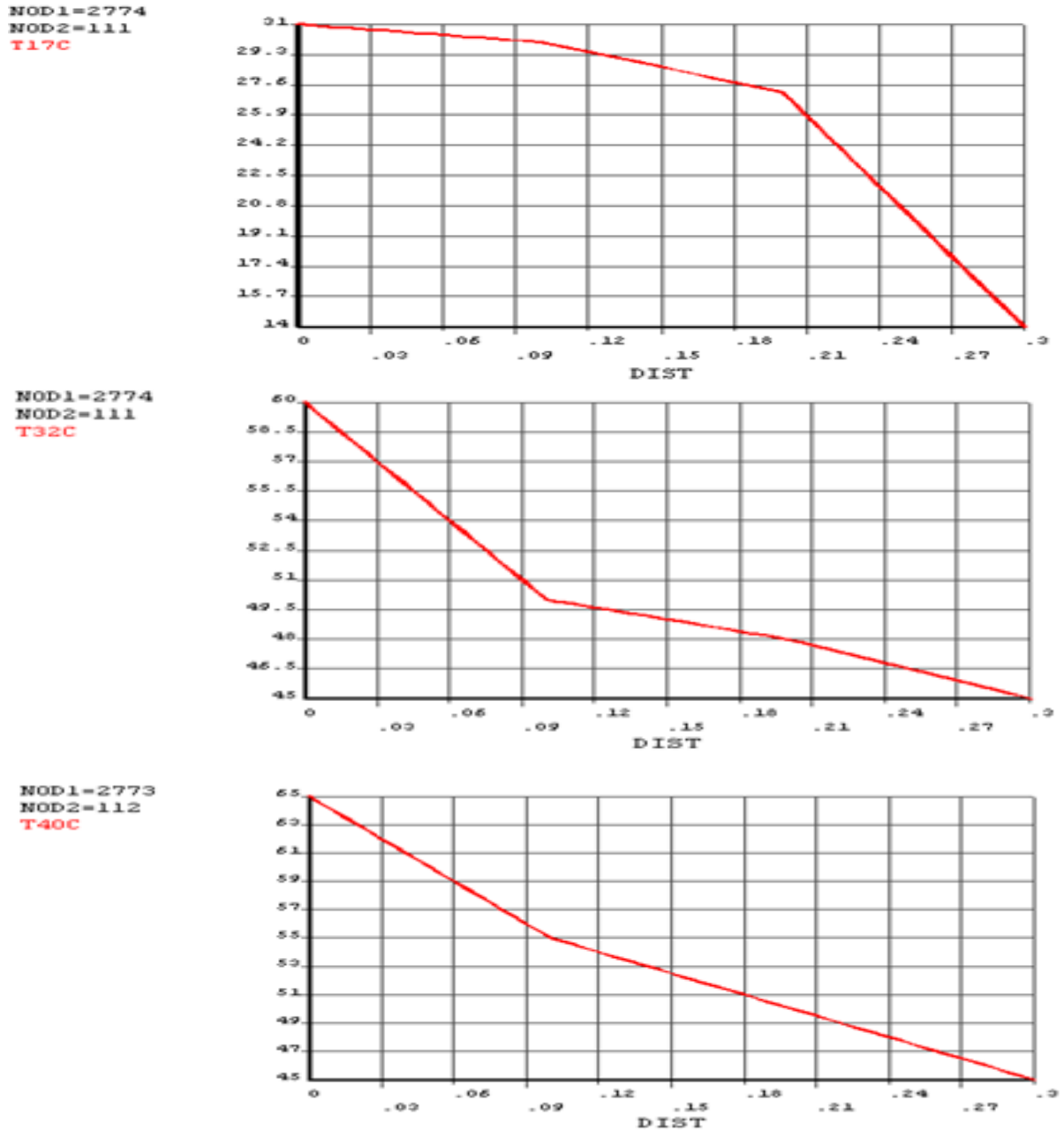
TBTEMP, 100

TBDATA,1, C1,C2,C3,C4

Figure 6. Variation des températures surfaciques en fonction de la profondeur du masque

TBOPT = 2 : Specifies the behavior law of model 2 namely (time hardening). This equation described the strain creep $(\dot{\varepsilon}_{cr})$ variation according to several parameters (C1, C2, C3, C4), such as the creep constants associated with the equation (4) bellow. Figure 7, illustrate the introduction of law creep procedure in the Ansys interface. In order to modeling the creep, the model used in our study is the model given in equation (4):

$$\varepsilon_{cr} = C_1 \sigma^{C_2} t^{C_3} e^{-C_4/T} \qquad (4)$$

With : ε_{cr} is the Creep strain, σ is the Equivalent stress, t represent the loading time, and C1, C2, C3, C4 : Creep parameters, giving as follows: C1 = 41.10-8 1/s, C2 = 1.48, C3 = -0.63, finally Tis the Medium temperature in Kelvin. Material is considered isotropic, and the basic solution method used is that of Newton-Raphson. This behavioral law is defined in ANSYS as "Time Hardening model"
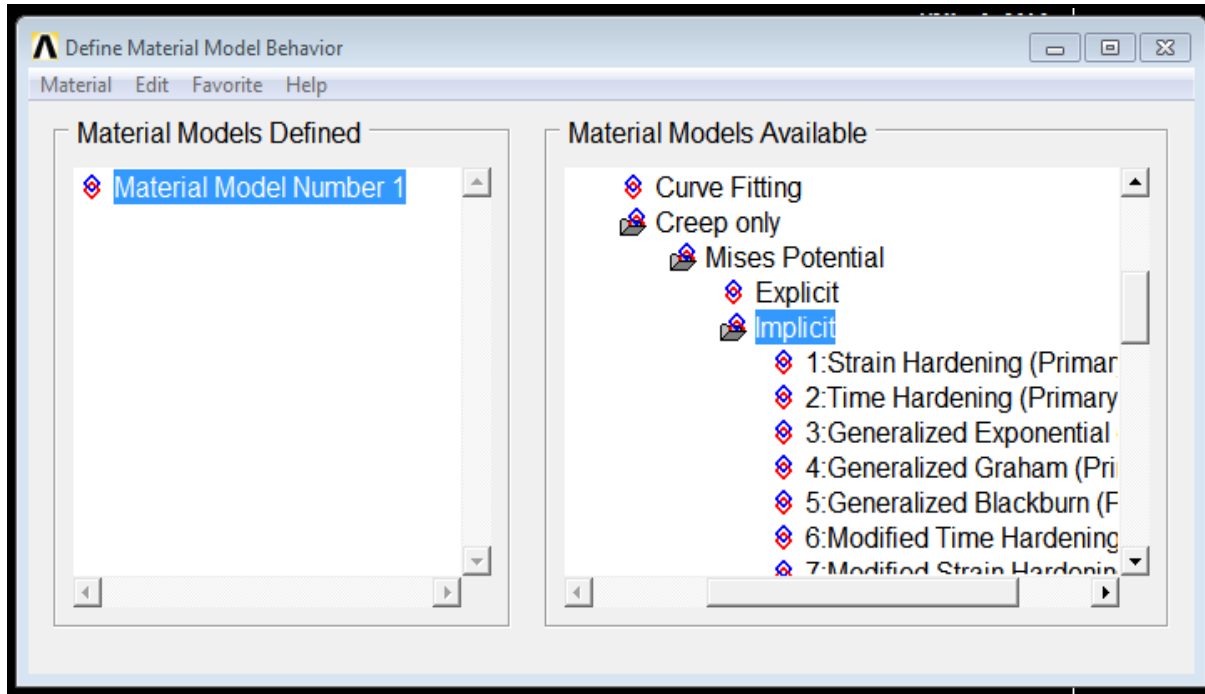
Figure 7. Interface introduction of the law creep model

Table 2. Surface mask temperature (Ts) and in the mask depth

Air temperature **(Ta)**	**17°C**		**32°C**		**40°C**	
	Eq (3)	Ansys	Eq (3)	Ansys	Eq (3)	Ansys
Ts at the mask surface	27°C	31°C	43°C	60°C	54°C	65°C
T° at 10cm of mask depth		29,5°C		50°C		55°C
T° at 20cm of mask depth		27.3°C		48°C		50°C
T° at 30cm of mask depth		14°C		45°C		47°C

Creep Phases

Under constant stress, the creep strain delayed is proportional to the load stress. It can therefore be classified as a "linear viscoelastic" material. Figure 8 bellow a curve typic of creep strain. We note thought the curve, three phases of creep, namely:

- Primary creep: represent the transient phase, during which the creep decreases with time, which corresponding to the material increase resistance.
- Secondary creep: corresponding to the phase stationary, or even quasi –viscous, during which the strain rate is constant over the time.
- Tertiary creep: in this phase, the strain rate grows until rupture.

From this figure, we see that the variation of "ε" and $\dot{\varepsilon}$ can be given by the following equation (5).

$$\varepsilon_{cr} = \varepsilon_0 + \varepsilon_1 + \varepsilon_2 + \varepsilon_3 + \varepsilon_4 \qquad (5)$$

With: ε_0: instantaneous deformation corresponding to the putting load, $\varepsilon_1 = At^x$: Primary creep with x < 1, ε_2 is the secondary creep wich is a linear function. $\varepsilon_3 = At^y$: Tertiary creep with y > 1

The function ε_2, ε_3 et ε_4, there are very large number of equations. The functions ε which describe the creep curves are the sum of power function with a linear and a logarithmic function.
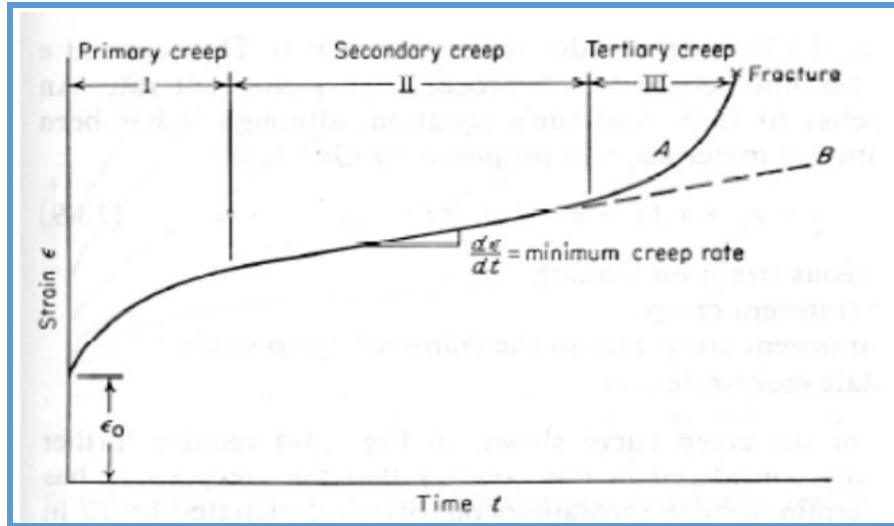
Figure 8. Creep curve typic under moderate load (1) and intense loading (2)
(Dieter, 1988, Ashby & Jones, 1991)

Primary Creep

Primary creep is commonly described as transient phase, where the creep rate decreases; Andrade's law models it as follows:

$$\varepsilon_{cr} = \varepsilon_0 + At^{1/q} \tag{6}$$

With: ε_0 represents instantaneous creep , A.t1/q Andrad's coefficient and q is a dimensionless constant (Andrade, 1910 and Andrade, 1914). (Nabarro, 1997) formulated a primary creep equation given as follow :

$$\varepsilon_{cr} = A\sigma^n t^m \tag{7}$$

With : σ (MPa) is the applied loading, A (MPa–nhr-m), n et m are temperature dependent constants (Pantelakis, 1983).7

Secondary Creep

The Norton's Power Law (Norton, 1929) describes the classical approach to the secondary creep model:

$$\dot{\varepsilon}_{cr} = A\sigma_{eq}^n \tag{8}$$

With: A et n are a creep secondary constants.

During the secondary creep, the strain creep continues to grow under constant stress, it does so at constant speed. Thus, it is identical to viscous flow and is usually referred to as viscous creep.

Tertiary Creep

Microstructural damage mechanism occurring during creep can be manifested in a number of ways, such as micro cracks, cavities, voids, etc. in increased scale. Typically, creep damage is classed into two forms: trans granular (ductile) damage and intergranular (brittle) damage. Trans granular (ductile) damage arises were slip bands of plasticity forming under high stress and low temperature. Intergranular (brittle) damage is a micro cracking process at grain boundaries under high temperature and low stress (Skrzypek, and Ganczarski, 1999). Damage is an all-inclusive non-recoverable accumulation that exhibits the same dependences as creep deformation: material behavior (i.e., creep constants), temperature, time, and stress. Generally, damage is

considered to be in continuum, (i.e., homogenous thought a body) thereby the expression continuum damage mechanics (CDM) is used. The damage phenomenon is closely aligned with the creep cracking and has been used to in local and nonlocal CDM approaches to predict creep crack growth. Many comprehensive lists of creep damage CDM-based formulations are available in literature (Skrzypek & Ganczarski, 1999; Lemaitre,1986). Early work in the characterization of creep damage by Kachanov (1967) and Rabotnov (1969), introduced the concept of scalar-valued damage evolution expressed as $\dot{\omega} = f(\sigma, \omega)$ where σ is uniaxial stress, is the current state damage. Damage is coupled within the creep strain rate via current damage and is expressed as $\dot{\varepsilon}_{cr} = f(\sigma, \omega)$. Within the creep strain equation, arises a net/effective stress which relates the physical space of damage where the presence of micro cracks and voids reduces creep strength, to an effective space, where microstructural creep damage is replaced with an effective increase in the applied stress

Results and Discussion

Figures 9, 10 and figure 11 illustrates the contour plot of creep strain ε_{cr}^{Y} and ε_{cr}^{X} and stress and stress of Von Mises in the structure dam and the upstream mask. The creep deformation results show that the creep curves are very spread in the plastic phase. The following equation allowed us to calculate the maximal plastic deformations$\left(\varepsilon_{x}^{p}, \varepsilon_{y}^{p}\right)$

$$\varepsilon_{cr} = \varepsilon_{el} + \varepsilon_{pl} \Rightarrow \varepsilon_{pl} = \varepsilon_{cr} - \varepsilon_{el}$$

Therefore, we will have as results:

$$\varepsilon_{x}^{p} = \varepsilon_{x}^{cr} - \varepsilon_{x}^{el} = 5.6207 - 0.1975 = 5.42355 \text{ mm/m}$$

$$\varepsilon_{y}^{p} = \varepsilon_{y}^{cr} - \varepsilon_{y}^{el} = 80.058 - 0.167 = 79.8913 \text{ mm/m}$$

Through the results, we see that the elastic deformation values $\varepsilon_{x}^{el}, \varepsilon_{y}^{el}$, remain low compared to the plastic deformations. Furthermore, the plastic deformations are macroscopically homogeneous. In other words, they reflect the fact that the upstream mask is uniformly deformed, we can conclude this:

- During the primary creep, there is mainly creation and propagation of dislocations. In general, these dislocations do not form particular cellular structures, they are entangled. We observe dislocations formed by sliding, deformation bands and slip lines more or less spaced depending on the applied loading (stress and temperature) and the creep time.
- During the secondary creep, the dislocations assemble to form a more or less clear cellular structure. These cells are less formed when the temperature is low.. They often show an elongation depending on the type of sliding activated. The dislocation density remains stable during this stage. The substructure is constantly being formed and destroyed: there is a equilibrium between the formation processes and annihilation of dislocations. In contrast, the disorientation between sub grains increases with time.

Temperature Effect on the Creep

The variation of creep strain (ε_{cr}) increases with temperature, it is thermally activated. it is follows an Arrhenius equation type:

$$\varepsilon_{cr} = Ae^{-\frac{Q}{RT}} \qquad (9)$$

whith: ε_{cr}: Creep strain during the secondary creep, A : Sinzing parameter, Q (J.Mol-1) : Activation energy, R : Gas Constant molar (8.314 J.mol^{-1}.K[-1]), T is Temperature in Kelvin, Figure 12 and 13 illustrates the creep strain curves under threes temperatures of 17°C, 32°C and 40°C respectively.

Effect of Temperature on Stresses

The following figures 14, 15 and figure 16 illustrates the temperature effect on the stress evolution over time, we constat that the stress evolution is carried in three phases:
The first phase speared over
a time interval of ($0 < t < 1000h$) were we note a stress maximal values of (σy), and a low values of elastic deformations. In this phase the upstream mask and the dam structure resist to the applied loads.
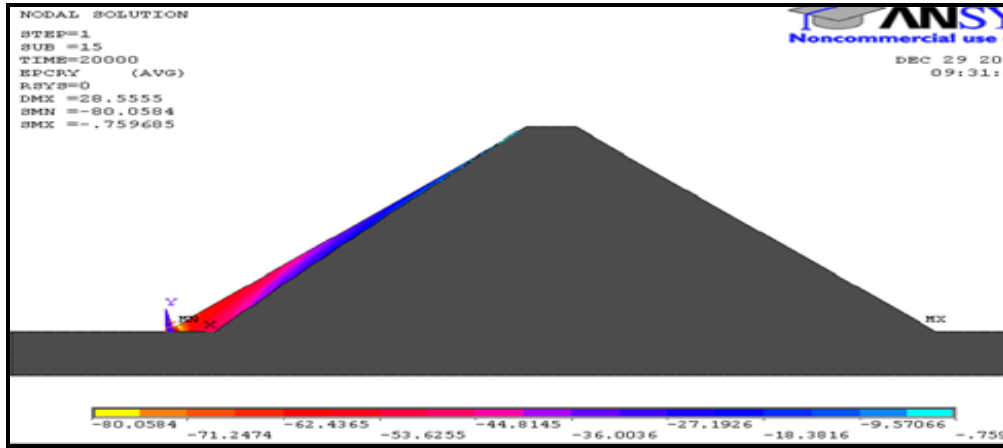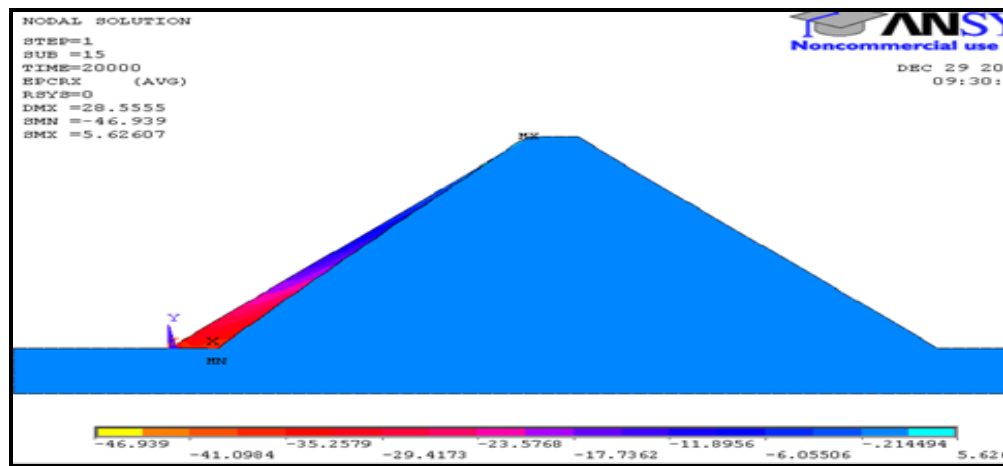
Figure 9. Creep strain contour plot (ε_{cr}^{y})

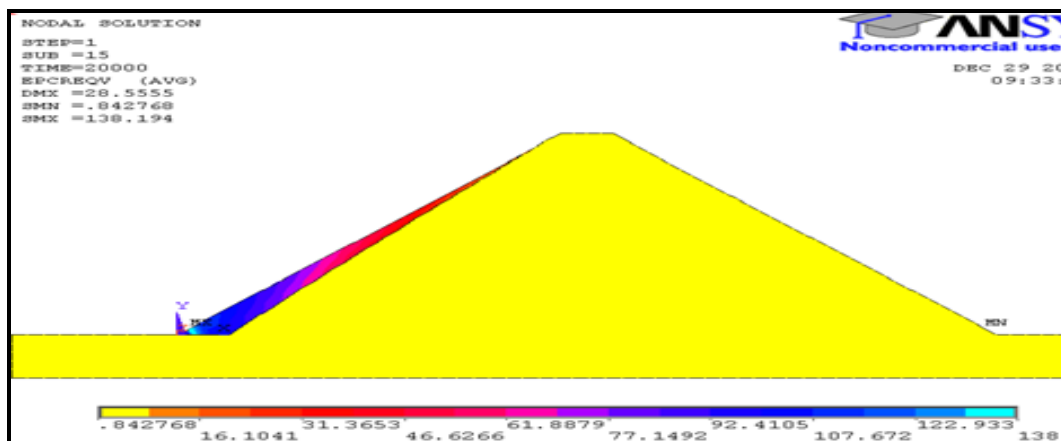Figure 10. Creep strain contour plot (ε_{cr}^{x})

Figure.11. Von Mises creep stress contour plot

In the second phase, the stress decreases slightly to remain constant over a time interval (1000h < t < 2500h), this is the start process of thermal activation. At the end phase, the stress decrease suddenly. The third stage, characterized by a progressive increase in the stress up to a value of 2000Pa. This phase corresponds to the phase of secondary creep or the speed of deformation remains constant and the material hardened (work hardening). At the time of this phase, dislocations are assembled to form cellular at least clear, that corresponds to a polygonization of the slip. The density of dislocations remains stable during this stage, on the other hand, confusion between under grains increases with time.
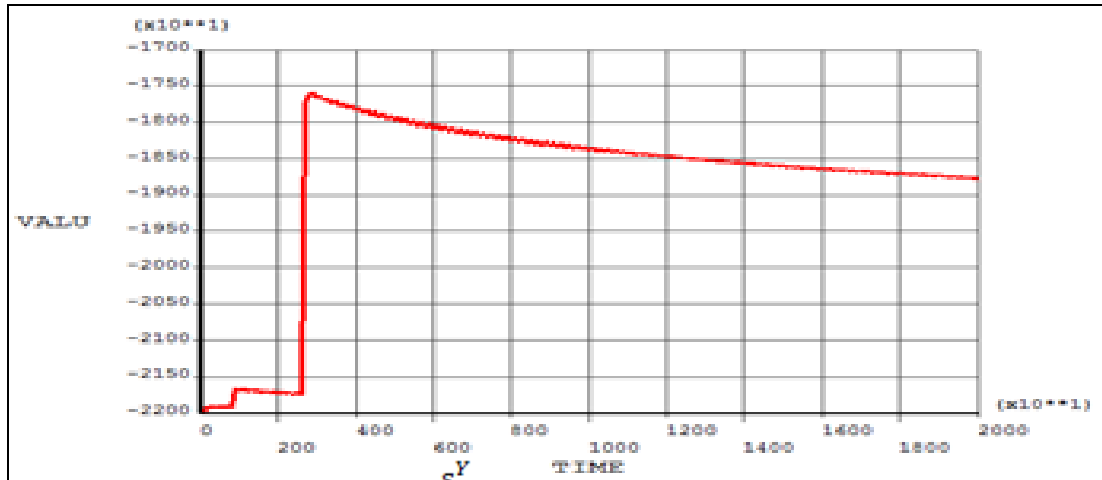
Figure.12.. Creep strain curve (ε_{cr}^{Y}) under three temperature 17°C, 32°C & 40°C
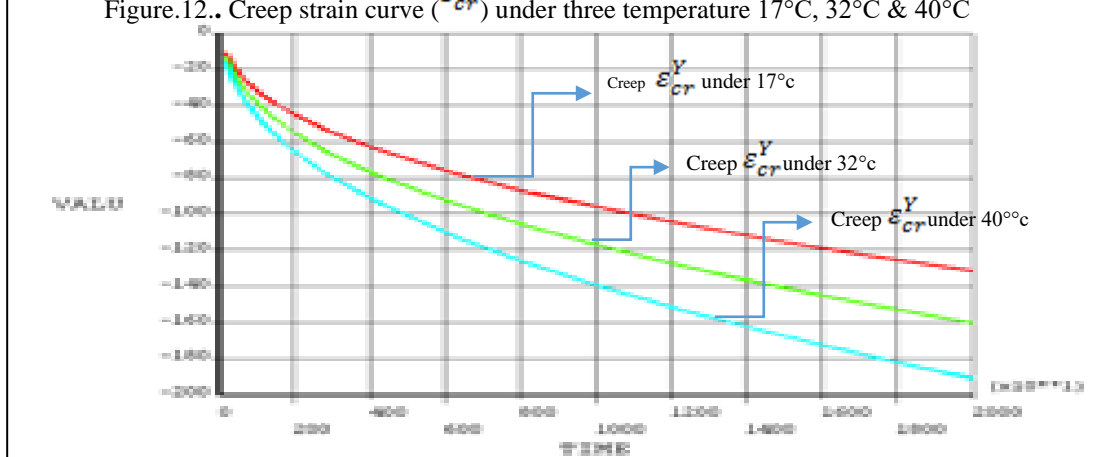
Figure13. Creep strain curve (ε_{cr}^{X}) under three temperature 17°C, 32°C & 40°C
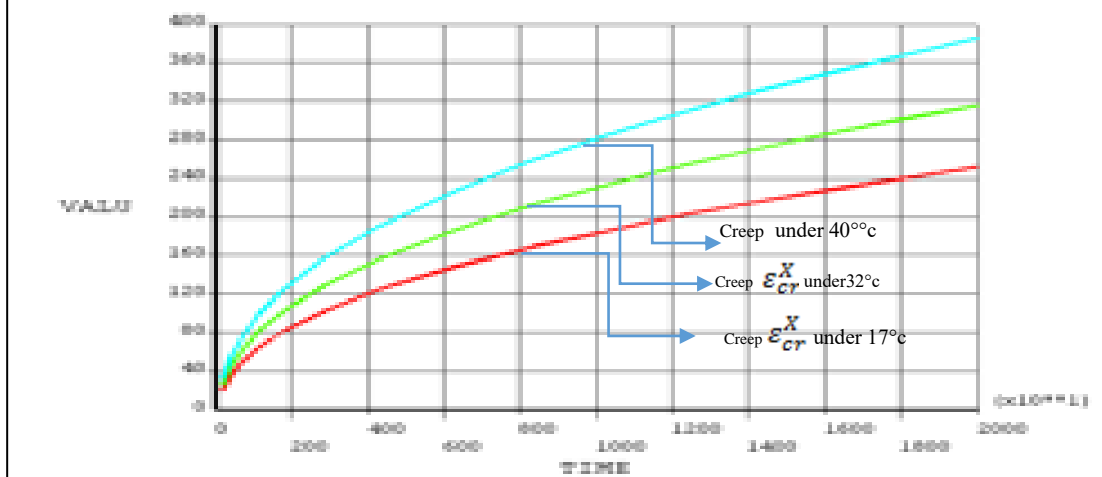
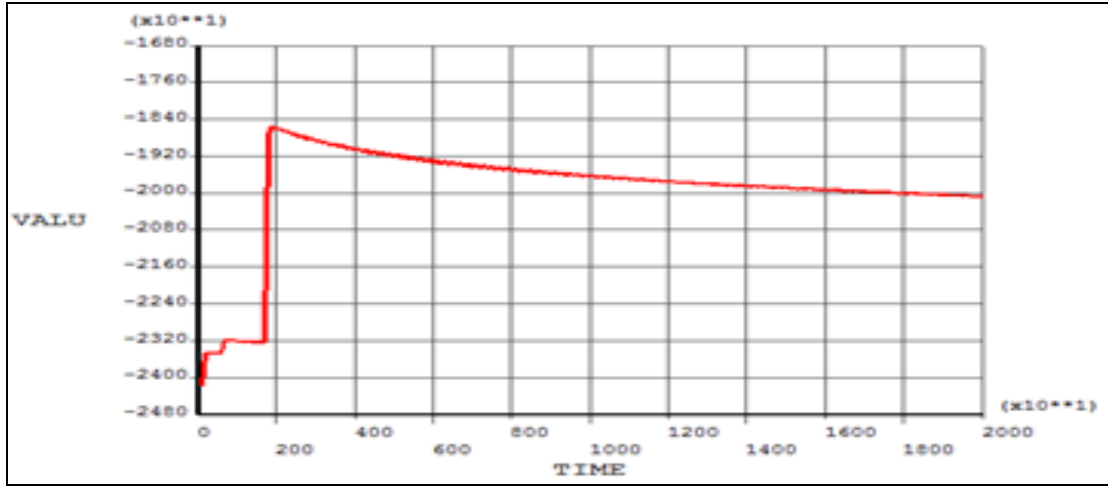Figure 14. σ_Y stress evolution under temperature of 17°C

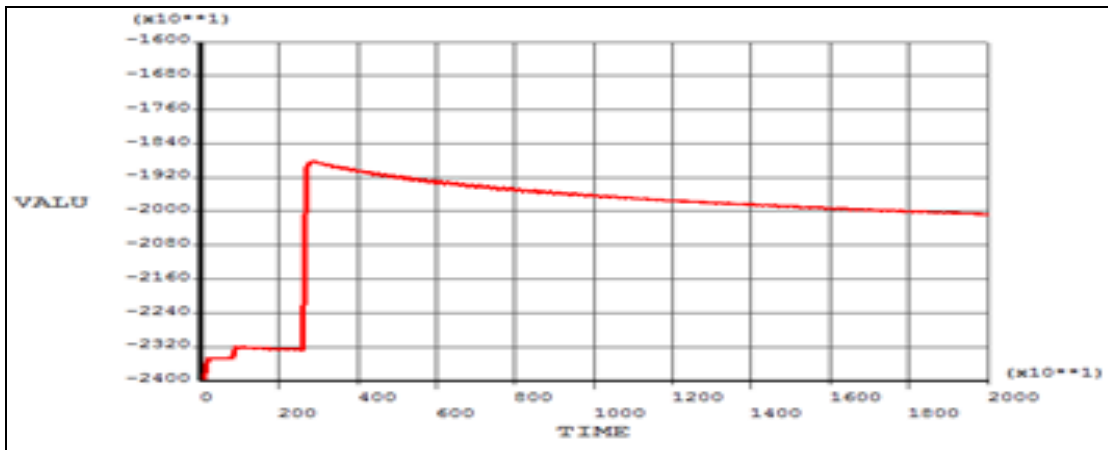Figure 15. σ_Y stress evolution under temperature of 32°C

Figure 16. σ_v stress evolution under temperature of 40°C

Conclusion

On a constaté à travers les résultats obtenus que le taux de déformations au fluage (ε_{cr}) atteint pratiquement 30% des déformations au bout d'un mois et 59% au bout de 6mois pour les différentes températures et chargement considérés. A 20000h du chargement constant, ces déformations atteignent une moyenne de 6.65 fois les déformations instantanées (ε_{el})

The objective of this study was to evaluate the stability of the bituminous concrete upstream mask in the rock-fill dams and to determine if it is possible to continue to build this type of mask upstream out of concrete the bituminous one on deposits of granular alluvia of average compactness in regions arid and semi-arid wine the temperature can reach the 60°C. The results obtained allowed to demonstrate the influence of temperature on the creep strain rate, and stress evolution applying the model of equation (4). It was found that the temperature increases the creep deformations, and the slope of the creep curve increases with the increase under temperature and we note through the results obtained that the rate of creep strain reached practically 30% of the deformations after one month and 59% after 6 months for the different temperatures and loading considered. At 20,000 hours of constant loading, these deformations reach an average of 6.65 times the instantaneous deformations.

The creep study, shows that the values of final creep are very important with high temperatures. The temperature of asphalt mixture has a great effect on deformation resistance ability, the higher the temperature, the more quickly the deformation resistance decrease. The total average deformations of creep reach 8,7 and 6 times the instantaneous strains for the temperatures of 17°c, 32°c and of 40°c respectively. Speeds of creep increase at the beginning of the loading and decrease then during time. The rate of viscous flow increases with the increase in viscosity λ and consequently the deformability of the binder increases. The increase in the

temperature has an impact on the parameters intrinsic of the asphaltic concrete, because they increase viscosity λ and decrease rigidity E.

Scientific Ethics Declaration

The authors declare that the scientific ethical and legal responsibility of this article published in EPSTEM Journal belongs to the authors.

Notes

This article was presented as a poster presentation at the International Conference on Technology, Engineering and Science (www.icontes.net) held in Antalya/Turkey on November 14-17, 2024.

References

Adam, K., Říha, J., & Špano, M. (2016). Investigation on the temperature of the asphalt-concrete facing of embankment dams. *International Journal of Pavement Research and Technology*, *9*(1), 73-81.

Andrade, E. N. D. C. (1910). On the viscous flow in metals, and allied phenomena. *Proceedings of the Royal Society of London. Series A, Containing Papers of a Mathematical and Physical Character*, *84*(567), 1-12.

Andrade, E. N. D. C. (1914). The flow in metals under large constant stresses. *Proceedings of the Royal Society of London. Series A, Containing Papers of a Mathematical and Physical Character*, *90*(619), 329-342.

ANSYS. (n.d.). *Element reference, general element features, 2.5. data tables-implicit analysis, 2.5.8 creep equations, ANSYS release 17.0 documentation*. Retrieved from https://www.ansys.com.

Ashby, M. F., Jones, D. R. H., & Bréchet, Y. (1996). *Matériaux: Propriétés et applications*. Paris: Dunod.

Betten, J. (2002). *Creep mechanics*. Springer.

Chebbah, L., Djemili, L., Bouziane, M. T., & Chiblak, M. (2020). Modélisation d'un masque en béton bitumineux (brut et protégé) sous sollicitations thermiques en régime transitoire. cas du masque de barrage Ghrib (Ain Defla, Algérie). *La Houille Blanche*, *106*(1), 42-49.

Chebbah, L. (2020). *L'Utilisation du béton bitumineux dans les travaux hydrauliques : Etanchéité des barrages en remblai* (p.175). Doctoral dissertation, Université de Biskra.

Dieter, G. E. (1988). *Mechanical metallurgy*. McGraw-Hill Book Company.

Djemili, L. (2006). *Critères de choix de projet des barrages en terre « étanchéité par le masque en béton bitumineux.* Doctoral dissertation, Université de Batna.

Djemili, L., & Chiblak, M. (2007). Study of the temperature distribution in the bituminous concrete facing used in fill dams in the region of west Algeria. *Journal of Engineering and Applied Science, 2*(3), 576–579.

Djemili, L., Behim, M., & Chiblak, M. (2012). Comportement du masque d'étanchéité du barrage Ghrib (Algérie) en absence de la protection thermique. *Courier du Savoir, 13*, 21–25.

Dougherty, D. J. (1996). Thermoplastic creep analysis using resin manufacturer's creep modulus data for thermoplastic joints. *ANSYS International Conference Proceedings*, 1359-1370.

Fadel, I. (2005). Asphalt mixture-designing basics in dams sealing–Designing of impermeable asphalt shell used in AL-Sorani dam. *Tishreen University Journal –Engineering Science Series, 27* (2), 23-38.

Garofalo, F. (1965). *Fundamentals of creep and creep-rupture in metals.* New York, NY: Macmillan.

George, K.P., & Husain, S. (1986). Thickness design for flexible pavement: A probablistic approach.' *Transportation Research Record, 1095*, 27-36.

Ghouilem, K. (2014). *Impact du fluage et de température sur les organes de lutte contre les infiltrations dans les barrages* (p.166). Doctoral dissertation, Université Mouloud Mammeri Tizi Ouzzou.

Kachanov, L. M. (1967). *The theory of creep, National Lending Library for Science and Technology Boston Spa, England.* Chaps. IX, X Boston Spa, England, Chaps. IX, X

Kraus, H. (1980). *Creep analysis.* NewYork, NY: John Wiley & Sons, Inc.

Nabarro, F. R. N. (1997). Thermal activation and andrade creep. *Philosophical Magazine Letters, 74*(4), pp 227-233.

Norton, F. H. (1929). *The creep of steel at high temperatures*. London: McGraw-Hill.

Odquist, F., & Hult, J. (1962*). Kriechfestigkeit metallischer Werkstoffe*, Springer Berlin.

Pantelakis, S. (1983). *Kriechverhalten metallischer werkstoffe bei zeitveranderlicher spannung*. Doctoral dissertation, RWTH Aachen University.

Rabotnov, Y. N. (1969). *Creep problems in structural members*, North Holland, Amsterdam

Skrzypek, J., & Ganczarski, A. (1999). *Modeling of material damage and failure of structures* (pp.69-78). Springer.

Trantina, G.G. (1986). *Creep analysis of polymer structures. Polymer Engineering and Science, 26*(11), 776-780.

Uzarowski, L. (2007). *The development of asphalt mix creep parameters and finite element modelling of asphalt rutting.* Doctoral dissertation, University of Waterloo.

Skrzypek, J., & Ganczarski, A. (1999). *Modeling of material damage and failure of structures* (pp.69-78). Springer.

Lemaitre, J. (1986). Local approach of fracture. *Engineering Fracture Mechanics, 25*(5-6), 523-537.

Mauduit, V., Mauduit, C., Greullet, N. V., Coulon, N., Hammoum, F., Hamon, D., ... & Chabot, A. (2013). Dégradation subite des enrobés bitumineux par période de gel/dégel: Analyse de cas de terrain et recherche exploratoire en laboratoire. *BLPC-Bulletin des Laboratoires des Ponts et Chaussées*, (279), 47.

National Agency of Dams and Transfers (ANBT). (2013). Execution study and monitoring of Souk N'Tleta dams construction in the wilaya of Tizi – Ouzou.

Lombari, L. (2005). *Bitume info manager, construire et innover* (p.36). Numéro Spécial Édition.

Rychen, R. (2013). *Impact du changement climatique sur les infrastructures routières – Analyse de risque et mesures d'adaptation*. Doctoral dissertation, EFPL

Incropera, FP., & DE WITT DP. (2002). *Introduction to heat transfer* (4th ed., pp.817-843). Wiley.

Author Information

Ghouilem Kamel
University Mouloud MAMMERI of Tizi - Ouzou
Ummto, BP 17 RP, Tizi-Ouzou 15000, Algeria
Contact e-mail: *kamel.ghouilem@ummto.dz*

Atlaoui Djamal
University Mouloud MAMMERI of Tizi - Ouzou
Ummto, BP 17 RP, Tizi-Ouzou 15000, Algeria

Merakeb Seddik
University Mouloud MAMMERI of Tizi - Ouzou
Ummto, BP 17 RP, Tizi-Ouzou 15000, Algeria

Mehaddene Rachid
University Mouloud MAMMERI of Tizi - Ouzou
Ummto, BP 17 RP, Tizi-Ouzou 15000, Algeria